# 10 • Optical methods for investigation of leaf photosynthesis

J.M. DUCRUET, M. BARON, E.H. DELUCIA, F. MORALES AND T.D. SHARKEY

## 10.1. OPTICAL METHODS

Light absorbed by chl. antenna is converted almost instantaneously into charge pairs in photochemical centres, which makes possible excitation by short flashes or modulated light thus generating various absorption, fluorescence or luminescence responses. The possibility of manipulating light excitation at will, together with the abundance of chromophores in the photosynthetic machinery, has favoured the development of optical monitoring of photosynthesis *in vivo*. The three complementary dimensions of optical methods, spectral, kinetic and imaging, provide unique tools to investigate the photosynthetic energy metabolism and, beyond, the bioenergetic status of the whole cell.

There is not a one-to-one correspondence between the measuring opportunities offered by various chromophores embedded in the thylakoid membranes and the aspects of the photosynthetic process they allow monitoring (Table 10.1). Starting from the mechanisms of light interactions with pigments, we will introduce the optical methods that have proved useful for studying leaf photosynthesis, using 'intensive' parameters (ratios such as $F_v/F_m$, kinetic amplitudes and time constants) that automatically compensate for variations of signal intensity between leaf samples. Other non-photosynthetic optical methods that can be used simultaneously (blue-green fluorescence (BGF), IR reflectance) will be briefly mentioned. Applications of leaf reflectance and fluorescence to remote sensing will be addressed in more detail in Chapter 15 and light absorption by leaves and canopies in Chapter 16.

## 10.2. ABSORPTION AND REFLECTION OF LEAVES

### 10.2.1. Leaf optics

Leaves have evolved to maximise light capture under most conditions, and a number of properties of leaves are related to this. Perhaps most striking is the common bifacial leaf in which the 'top' (usually the adaxial surface) has palisade cells that form light guides between them, whereas the 'bottom' (usually abaxial) surface has spongy mesophyll cells that maximise light scattering (Fig. 10.1A). This arrangement enhances light penetration from the top through the palisade layer, but enhances absorption of light that gets into the spongy layer. This effect works for collimated light like that experienced by leaves in direct sunlight. However, it does not work for diffuse radiation found in understories. Not surprisingly leaves exposed to full sun often have very distinct palisade layers while leaves in shade environments may have little or no palisade layer, even when they are from the same plant.

As a result of the internal structures of leaves, light being reflected from the top of a leaf may have travelled through the palisade layer, been scattered in the spongy layer and travelled through the palisade layer again. Light reflected from the bottom of a leaf may be reflected from much shallower regions as it encounters the scattering spongy layer as soon as it gets through the epidermis. Many leaves look much lighter on the bottom than the top because of the enhanced scattering in the spongy mesophyll layer (Vogelmann, 1993). The lighter appearance indicates greater reflectance, for example, a leaf of *Xanthium strumarium* was found to have a reflectance of 6% of 681 nm light from the adaxial surface, but 10% from the abaxial surface. Transmissivity was not affected by whether the light was adaxial or abaxial, and so the difference in reflectivity indicated a difference in absorptivity, 88.5% when illuminated on the adaxial surface but just 84.5% when illuminated on the abaxial surface (Sharkey, 1979). This demonstrates the utility of the internal structure of leaves for increasing light absorption.

The light scattering in the mesophyll layer, and to a lesser extent scattering caused by structures within cells,

*Terrestrial Photosynthesis in a Changing Environment: A Molecular, Physiological and Ecological Approach*, ed. J. Flexas, F. Loreto and H. Medrano. Published by Cambridge University Press. 

Table 10.1 *Optical methods and the photosynthetic mechanisms they allow to monitor in leaves. X: relevant. (X): indirect indication.*

*The corresponding sub-chapters are indicated in the first column.* **PSII, PSI***: intrinsic properties of the photosystems and alterations by stresses.* **PSI, PSI ET***: electron transfer through illuminated photosystems. Particular excitation wavelengths can be used to favour PSII (blue 480 nm) or PSI (far-red > 700nm) activity.* **PMF***: Proton Motive Force. The two components* **ΔpH** *(thylakoid transmembrane proton gradient) and ΔΨ (thylakoid transmembrane electric field) can be selectively monitored. Under illumination, the pH can reach 7.8 in the stroma and 4.5 in the lumen. A residual ΔpH can remain in the dark, maintained by a chlororespiratory electron flow.* **AP***: Assimilatory potential NADPH + ATP in equilibrium with the pool of triose-phosphates (Gerst et al., 1994).* **ST***: State transitions, state 1 to state 2 corresponds to the migration of the peripheral antenna of PSII towards PSI. State 2 favours CEFI.* **CEFI***: electron transfer around PSI under light, generates ATP only.* **Ind CEFI, CR***: induction of CEFI pathways, chlororespiration. The cyclic pathway(s) around PSI may be open although there is no electron flow in absence of light. This induction can be monitored in the dark by a weak electron transfer, closely related to chlororespiration (from stroma to PQ pool).* **Thylakoid membrane***: these lipids are highly unsaturated, which contributes to the membrane leakiness to protons (measured by green light absorption), to the heat sensitivity of PSII (curves $F_0/T$) and to lipid peroxidation (High temperature ThermoLuminescence).* **Commercial instruments***: commercially available optical instruments dedicated to photosynthesis research.*

| | | PSII | PSII ET | PSI | PSI ET | PMF: ΔpH | PMF: ΔΨ | AP | ST | CEFI | Ind. CEF1 CR | Thylakoid membrane | Commercial instruments |
|---|---|---|---|---|---|---|---|---|---|---|---|---|---|
| **Absorption and related** | | | | | | | | | | | | | |
| 1.2 | P700 (A820) | | | X | X | | | (X) (light) | | X (light) | X (dark) | | H W B |
| 1.3 | Green 505–518–535 | | | | | X | X | | | (X) | | X Leak | W B |
| 1.4 | PRI | | (X) | | (X) | (X) | (X) | | | | | | P S |
| 1.5 | NADPH (F500) | | | | | | | X | | | | | W |
| 1.6 | Photoacoustic Spectroscopy | X | X | X | X | | | | X | X | X | | |
| **Chlorophyll fluorescence** | | | | | | | | | | | | | |
| 2.1 | spectra | X | | X | | | | | X | | | | B |
| 2.2 | lifetime | X | X | X | | | | | | | | | |
| 2.3 | 0→P | X | | | | | | | | | | | B H O P Q W |
| 2.4 | Modulated | X | X | | | X (qE) | | | X (qT) | | | | H L O P W Q T |
| 2.5 | $F_0$ | X | | | | | | | | | X $F_0$/t | X $F_0$/T | → id |
| **Chlorophyll luminescence** | | | | | | | | | | | | | |
| 3.1 | DL | X | | | | X (dark) | | | | | | | |
| 3.2 | TL (A,Q,B,C) | X | | | | (X) (dark) | | | | | | | F P Q |
| 3.3 | Afterglow (AG) | | | | | | | X | | ( X) | X | | → id |
| 3.4 | Modulated (DLE) | X | | | | X (light) | X (light) | | | | | | H |
| 3.5 | HTL bands | | | | | | | | | | | X Peroxid. | F |

Commercial instruments for photosynthesis. B: www.bio-logic.info, F: www.fan-gmbh.de, H: www.hansatech-instruments.com, L: www.licor.com O: www.optisci.com, P: www.psi.cz, Q: www.qubitsystems.com, S: www.skyeinstruments.com, T: www.technologica.co.uk, W: www.walz.com

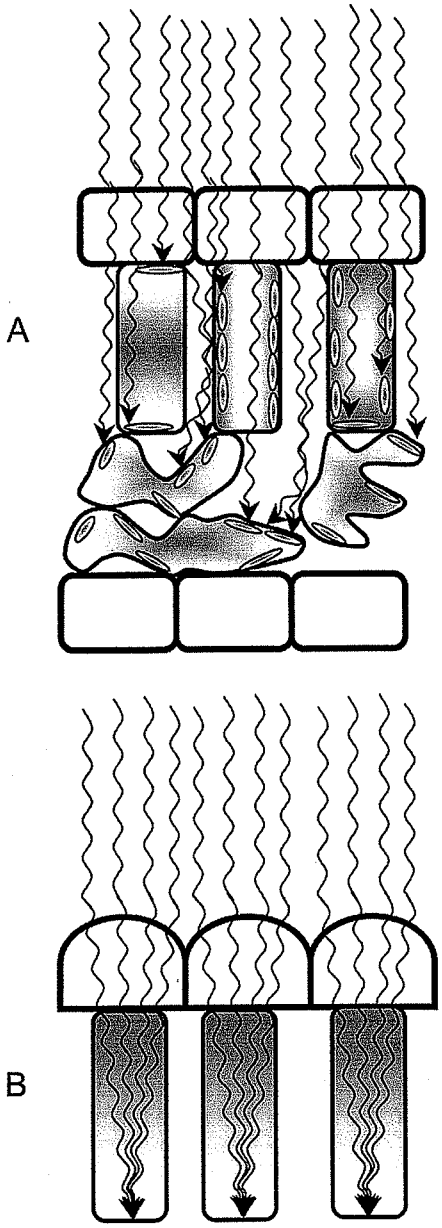


Fig. 10.1. Leaf optics. (A) Light paths through leaves. Light rays that pass through the epidermis and encounter the space between palisade cells will pass through the upper layer of the leaf. The irregular shapes of the spongy cells will maximise the chance that light will enter a cell. The spaces between the palisade cells will act as light guides because the large difference in index of refraction will cause light to reflect if it hits at a shallow angle (as depicted in the space between the left and centre palisade cell). Light that reflects off one spongy mesophyll cell is likely to hit another cell at a steep angle and so enter the cell. Chloroplast position can also affect light absorption. If all chloroplasts are along the anticlinal walls, the centre of a palisade cell can act as a light guide, just like the spaces between the palisade cells (shown in centre palisade cell). In addition to the light-guide effect, the fact that essentially all of the absorbing material (e.g., chlorophyll) is located in relatively small spaces (chloroplasts) gives rise to the sieve effect. (B) Epidermal lensing. Parallel light rays can be concentrated in some regions of the mesophyll cells because the shape of epidermal cells can cause them to act as lenses. The advantage of increasing the non-uniformity of light distribution through the leaf is not clear (Brodersen and Vogelmann, 2007).

can increase the effective pathlength of light as it travels through a leaf. The effect is strongest for leaves with low concentrations of chl. and for wavelengths that are not strongly absorbed. Thus, for blue or red light the effective pathlength may by roughly the same as the depth of the leaf, whereas for green light the effective pathlength may be five times greater than the depth of the leaf (Vogelmann, 1993). One result of this arrangement is that photosynthesis at different depths in the leaf may be driven by different light quality, with green light extending deeper into the leaf than red or blue (Terashima *et al.*, 2009).

Leaf epidermal cells are often curved, concentrating light within leaves (Fig. 10.1B). However, the advantage of concentrating light is not clear as high light levels in some regions would be balanced by low light elsewhere in the leaf. Another possibility is that the lens-shaped epidermal cells might enhance penetration of light coming from low angles into the leaf, but experimental evidence does not support this view (Brodersen and Vogelmann, 2007). These effects and others will affect the optical methods used to probe photosynthesis. For example, fluorescence from leaves will come from superficial layers of the leaf, whereas $CO_2$ fixation will be an average for all cell layers (Peguero-Pina *et al.*, 2009, and references therein; see also Chapter 16).

Absorption (Section 10.2) is classically measured as transmittance through the leaf, absorptance being defined as $\log_{10}(1/\text{transmittance})$, whereas fluorescence (Section 10.3) and luminescence (Section 10.4) are measured from the illuminated side. However, taking advantage of light diffusion by leaf tissues, absorption can be detected as reflectance, i.e., light diffused backwards for experimental convenience (e.g., using multifurcated light guides). Because light is strongly absorbed and re-absorbed in the blue and red absorption bands of chl. and diffused, even more transmitted light can be detected in leaves mainly in the near IR (P700 measured at 820 nm) and green (505 nm, 518 nm, 535 nm, (PRI))

spectral regions. Photoacoustic spectroscopy also relies on light absorption, but detection by sound emission is quite different.

### 10.2.2. Absorption of P700 (820 nm): redox kinetics of the photosystem I centre

Photochemical charge separation, produced by a quantum of light energy absorbed in the pigment antenna and migrating randomly to a photochemical centre, consists of the transfer of an electron from the excited reaction centre chl. molecule to a primary acceptor:

$$Chl^{*} + A \rightarrow Chl^{+} + A^{-} \qquad \text{[Eqn. 10.1]}$$

The transient $Chl^{+}$ cation (more exactly a positive charge delocalised over a chl. dimer) is rapidly re-reduced by a primary electron donor. These redox changes result in an absorption change at 680 nm for PSII (P680) and 700 nm for PSI (P700), and increased absorption band around 820 nm that offers the experimental advantage of being outside the domain of strong chl. absorption.

The transiently oxidised primary donor $P680^{+}$ in PSII is re-reduced to P680 in the nanosecond range by the closely bound primary donor tyrosine Z, producing the high fluorescence state $P680Q_A^{-}$, the origin of variable fluorescence (Chl-F: see Section 10.3 and Chapter 2). In contrast, in PSI, $P700^{+}$ being re-reduced by a mobile plastocyanin molecule in the lumen has a longer lifetime, in the microsecond range, whereas the primary acceptor $A_0^{-}$ is rapidly reoxidised by the secondary acceptor $A_1$, resulting in $P700^{+}A_0$. No variable fluorescence arises from PSI. The electron produced by the charge separation is transferred through protein-bound electron carriers to a ferredoxin (Fd) molecule soluble in the stroma. This gives rise to the common practice of using fluorescence to study PSII, but absorbance at 820 nm to study PSI.

Absorbance changes at 820 nm, outside bulk chl. absorption, primarily reflect $P700 \leftrightarrow P700^{+}$ oxydoreduction, but this 820 nm secondary band of P700 overlaps with the broad absorption band of plastocyanin: reduced noise and improved specificity for P700 can be attained using a dual-wavelength differential detection system. The ratio of $P700^{+}/P700$ reflects the photochemical activity of PSI under steady state illumination (Schreiber *et al.*, 1989). In the dark, P700 is fully reduced. It can be fully oxidised into $P700^{+}$ by a light-saturating pulse when the donation of electrons by plastocyanin to $P700^{+}$ is the limiting step (donor-side limitation). However, the turnover of PSI can be also acceptor-side limited, for example, after inactivation of the Calvin cycle by a period of darkness, and the total amount of P700 has then to be assessed by a combination of far-red (FR) illumination and saturating pulse (Klughammer and Schreiber, 1994). Three relative values of P700 absorbance measured by an unactinic 820 nm light, first without, then with actinic light and finally during a saturating pulse, are needed to determine the $P700^{+}/P700$ ratio under a steady state illumination, in order to calculate the electron-transfer activity of PSI.

Cyclic electron flow around PSI was discovered *in vitro* by Arnon (1959), but its role *in vivo* has been questioned until optical methods (mainly P700 absorption and photoacoustic spectroscopy (Section 10.2.6), more indirectly basal Chl-F $F_0$ and luminescence increase in darkness) made its monitoring in leaves possible. This has provided evidence for the roles of CEFI in various stress situations: (1) enhancing the protective NPQ of fluorescence by increased proton pumping into the lumen (Section 10.3.4); and (2) provision of additional ATP for protein synthesis and repair (Rumeau *et al.*, 2007). The molecular basis of CEFI are still partly unknown (Chapters 2 and 3, review by Shikanai, 2007).

An important tool for detecting an induction of CEFI is provided by kinetics of $P700^{+}$ re-reduction in the dark immediately after an illumination. After white light, dark reduction of $P700^{+}$ is multiphasic, with fast phases down to the sub-ms range corresponding to electron flow from PSII (Govindachary *et al.*, 2007; Baker *et al.*, 2007). As FR light (>700 nm) excites PSI at a greater extent than PSII, it can be used to favour PSI activity. Kinetics of $P700^{+}$ reduction after FR light are slower than after white light, and consist of two phases with $t_{1/2}$ around ~2 s and ~12 s and a 2:3–1:3 ratio of amplitudes respectively (Cornic *et al.*, 2000; Fig. 10.2A,B). A faster phase (~100 ms) emerges after a time of dark adaptation corresponding to the inactivation of the Calvin cycle (Chow and Hope, 2004); it can be ascribed to a cyclic "overflow" of electrons from the over-reduced PSI acceptor pool to P700+ (Breyton *et al.*, 2006). An acceleration up to fivefold of $P700^{+}$ biphasic (2s and 12s) reduction occurs in conditions that trigger the pathway(s) for CEFI (pre-illumination by high-intensity white light, anoxia, warming, etc): electrons coming from reductants stored in the stroma are enabled to flow to the intersystem chain, then reduce $P700^{+}$ (Fig. 10.2). A faster $P700^{+}$ reduction in the dark indicates that cyclic pathway(s) are open, even though the actual electron flow is very weak in the absence of light. $P700^{+}$ reduction rate can also be recorded under continous illumination during 100 ms dark intervals (Golding and Johnson, 2003).

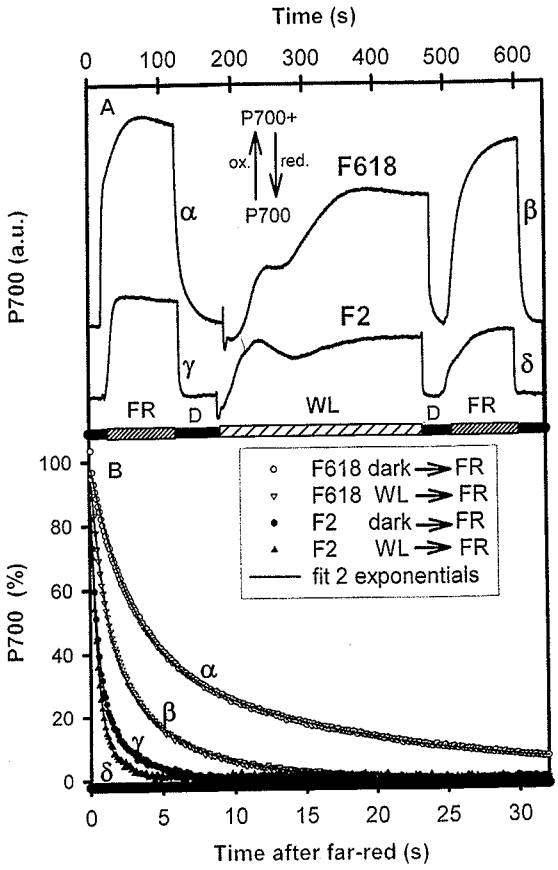


Fig. 10.2. P700 oxidation by far-red (FR) or white light (WL) and re-reduction in the dark (D), monitored by absorption at 820 nm. F618 and F2 maize inbred lines, sensitive and tolerant to chilling temperatures, resp. Plants transferred from illuminated growth chamber (17°C, 290 μmol $m^{-2}$ $s^{-1}$) were maintained in darkness for 1 h. Measurements on attached leaves at an approximate 21°C room temperature. (A) P700 redox kinetics during a light sequence: dark → 100s FR → dark → 5min WL → dark →100s FR → dark. Kinetics α – δ are enlarged in B. (B) Reduction kinetics following 100 s FR, before and after 5 min white light, fitted by two exponentials. From Ducruet *et al.* (2005) with permission.

The pathways that support an ATP-generating CEFI in the light (review by Bukhov and Carpentier, 2004) may be shared by a chlororespiratory electron flow in the dark from stroma reductants to the PQ pool, subsequently reoxidised by oxygen through a plastidial terminal oxidase (PTOX) (review by Peltier and Cournac, 2002). This stroma-to-PQ part of the chlororespiratory pathway can be investigated by the same methods as CEFI.

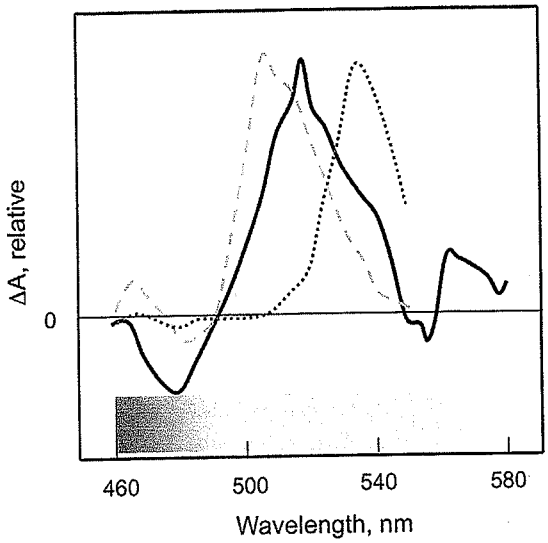


Fig. 10.3. Absorbance phenomena observable in green wavelengths. The solid line is the absorption spectrum for the electrochromic shift, the dashed line is the absorbance change caused by zeaxanthin formation and the dotted line is the absorption change caused by chloroplast swelling. Data are taken from Wise and Ort (1989), Bilger *et al.* (1989).

Activity of CEFI (and also CEFII) can also be deduced from the difference between PSI and PSII electron transfer, monitored by P700 absorption and Chl-F (Section 10.3.4), respectively, on the same leaf spot.

### 10.2.3. Green-light absorption methods.

Changes in optical density (absorbance [A] or extinction [E]) in the green region of the spectrum can give information about several different photosynthetic processes. Three signals that can be distinguished are the electrochromic shift (ECS) reflecting the electrical potential of the thylakoid membrane, light scattering, reflecting chloroplast swelling and chloroplast movement and the formation of zeaxanthin.

The ECS was discovered by Junge and Witt (1968). They found that absorption changes centred at 518 nm (ΔA518) were linearly related to the transthylakoid electrical potential (ΔΨ). These changes come about because the electric field changes the absorption spectrum of carotenoids. Although the effect is small, at the steeply declining slope of the absorption spectrum, around 518 nm, the change in optical density is easily measured (Fig. 10.3).

The ΔA518 measurement can be made with dark-adapted leaves to obtain information on the efficiency of PSII and the integrity of the thylakoid membrane. In dark-adapted leaves the ATP synthase is fully deactivated and the ΔΨ resulting from a very brief flash of light is dissipated through leakiness of the membrane. Wise and Ort (1989) used ΔA518 (referenced to 540 nm) to show that chilling reduced the efficiency of PSII without affecting membrane integrity. Ortiz-Lopez *et al.* (1991) used it to show that photophosphorylation is not impaired by water stress in field-grown sunflowers. Schrader *et al.* (2004) used ΔA518 measurements with heat-stressed leaves to show the opposite, that heating compromised membrane integrity before reducing PSII efficiency.

In light-adapted leaves the ΔA518 is measured during short dark intervals, and the technique has been called dark interval relaxation kinetics (DIRK) (Sacksteder and Kramer, 2000). The $DIRK_{ECS}$ reflects the steady state *pmf* and the rate of proton flux through the ATP synthase. When actinic light is turned off the *pmf* continues to drive protons through the ATP synthase until the entire *pmf* has been dissipated (strictly speaking, until the *pmf* equals the ΔG of ATP formation). The ΔΨ plus the ΔpH make up the *pmf*. Ion movements that occur in light-adapted leaves can convert some of the *pmf* from ΔΨ to ΔpH. After darkening a leaf, the *pmf* is dissipated in approximately 30 ms, while the ΔpH component relaxes over several seconds reversing the ECS signal (Baker *et al.*, 2007). Therefore, the rapid decline in the ECS signal following darkening reflects the total *pmf*, whereas the subsequent reverse ECS reflects the ΔpH. The difference is the ΔΨ (Baker *et al.*, 2007). The ECS signal is very rapid, and the measure of *pmf* can be made simply by measuring the absorbance at 518 nm. This technique has now been used to investigate both water stress and heat stress on the proton fluxes in PET (Kohzuma, *et al.*, 2009; Zhang and Sharkey, 2009; Zhang *et al.*, 2009c).

However, other changes in the green absorption spectrum are much larger (>0.1 OD[1] are common) than the ECS signal (commonly <0.01 OD), and so even though much slower, measuring the partitioning of *pmf* between ΔΨ and ΔpH requires measuring at at least two wavelengths, and it is even better to measure at three wavelengths (505 nm for zeaxanthin changes, 518 nm for ECS, and 535 nm for scattering changes; Fig. 10.3).

In intact leaves large absorption changes in the green (and other wavelength ranges) can be caused by chloroplast movement (Wada *et al.*, 2003). *In vivo* (in chloroplasts and leaves), the light-minus-dark-difference absorption spectra have three peaks in green light, at 505 nm (with a shoulder at 535 nm), 468 nm and 437 nm (Yamamoto *et al.*, 1972; Morales *et al.*, 1990). These three peaks reflect the conversion of violaxanthin to zeaxanthin (Yamamoto *et al.*, 1972). The broad shoulder at 535 nm is likely caused by changes in light scattering related to ΔpH-mediated chloroplast changes. Light scattering caused by chloroplast swelling and/or thylakoid stacking, may be related to the ΔpH component of the *pmf* (Crofts *et al.*, 1967; Deamer *et al.*, 1967; Heber, 1969). Changes in the aggregation state of antenna pigment-protein complexes mediated by an accumulation of de-epoxidised forms of the xanthophyll-cycle molecules (Gamon *et al.*, 1990; Morales *et al.*, 1990; Ruban *et al.*, 1993) can also influence the light-scattering effect seen at 535 nm. The details of the causes of chloroplast swelling and shrinking remains under debate (Ruban *et al.*, 2002).

These effects (plus other minor absorption changes in the green) vary in extent and speed of change. The ECS change generally can be measured over hundreds of milliseconds but, over seconds, the much larger changes of chloroplast movement and chloroplast swelling and shrinking can overwhelm the ECS signal. A two-wavelength system, with an additional third reference wavelength, is now commercially available (emitter unit DUAL-EP515 and the detector unit DUAL-DP515, Heinz Walz GmbH, Effeltrich, Germany), but three measuring wavelengths are needed to accurately separate the different effects that give rise to changes in green-light absorption of leaves.

### 10.2.4. Photosynthetic reflectance indexes

Chlorophyll fluorescence (see Section 10.3 and Chapter 16) is an intrinsic probe of photosynthetic efficiency. However, crop biomass is not only determined by leaf photosynthetic activity but by other factors as well, such as PAR absorbed and leaf area index (LAI). In many cases, in response to environmental factors, leaf growth stops before leaf photosynthesis is affected. Therefore, a convincing global indicator of the physiological state of plants should be able to monitor simultaneously both photosynthetic efficiency and

[1] OD (Optical density) or sometimes *E* (extinction) is the measure of absorptivity from the Beer-Lambert equation, $OD = \log_{10}(I_0/I_1)$, where $I_0$ is the light intensity coming into the system (e.g., the leaf) and $I_1$ is the light intensity coming out of the system. If a leaf absorbs 90% of the incoming light the OD is one, for 99% absorption the OD is two.

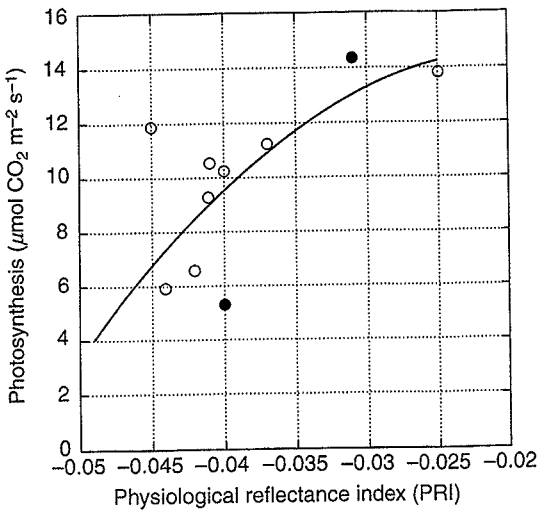


Fig. 10.4. Relationship between the physiological reflectance index (PRI) and photosynthesis. Kermes oak seedlings experiencing a progressive drought stress (open circles) and during two different days after re-irrigation (solid circles). From Peguero-Pina *et al.* (2008).

leaf growth. This can be achieved measuring hyper or multi-spectral reflectance in the visible area, where both normalised difference vegetation index (NDVI) and PRI can be obtained by using hyper-spectral or, at least, multi-spectral reflectance.

With the development of hyper-spectral reflectance in the 1990s, it has become possible to quantify simultaneously different leaf properties, including those related to photosynthesis (greenness, ie., chl. concentration, photosynthetic efficiency, etc.) (Gamon *et al.*, 1990; Peguero-Pina *et al.*, 2008). Several vegetation-monitoring techniques have been developed to quantify green vegetation and to map its spatial distribution, with the aim of estimating canopy photosynthesis and/or net primary productivity (NPP) (Grace *et al.*, 2007). Many vegetation studies were focused to detect only canopy greenness (e.g., NDVI=(R750−R705)/(R750+R705), where R750 and R705 represent reflectance at 750 and 705 nm, respectively). NDVI is not necessarily a good indicator of crop physiology because cessation of leaf growth and impaired photosynthetic rates often occur before chl. net destruction (see Chapter 15).

The so-called PRI=(R531−R570)/(R531+R570), where R531 and R570 are reflectance signals at 531 and 570 nm respectively, may be used to monitor photosynthetic dynamic changes (Fig. 10.4), with reflectance sensors designed to measure at certain distances (Evain *et al.*, 2004). Thus, PRI provides a quick and non-destructive assessment of leaf and canopy physiological properties (Evain *et al.*, 2004; Louis *et al.*, 2005) for a wide range of species (Gamon *et al.*, 1997). The physiological bases for PRI changes began to be investigated in the 1990s (see Section 10.2.3). Rapid vegetation reflectance changes around 531 nm (PRI changes) owing to sudden changes in incident light or upon imposition of a given stress condition could be sensed remotely and passively using a portable radiometer (Peguero-Pina *et al.*, 2008). PRI changes have been shown to correlate well with other photosynthetic activity parameters such as NPQ, the stationary fluorescence level $F_s$ (Section 10.3.4) and de-epoxidation state of the xanthophyll cycle (Peguero-Pina *et al.*, 2008), and proved to be a good indicator of the increasing $CO_2$ assimilation of a pine forest during spring (Louis *et al.*, 2005) or of water stress level (Peguero-Pina *et al.*, 2008).

In contrast to the three green absorption signals described above (Section 10.2.4) that vary in the sub-second/second range and return specific information, the PRI is a global indicator of photosynthetic activity, varying within seconds/minutes. PRI measurements can be done by clipping the leaf or remotely.

Other simple reflectance indices have been proposed to estimate photosynthetic activity and to track plant stress. Dobrowski *et al.* (2005) reported that R690/R600 and R740/R800 correlated well with $F_s$ and $CO_2$ assimilation rate in a water-stress experiment. Obviously, reflectance at 690 and 740 nm contains Chl-F, and therefore correlation with other photosynthetic parameters is not surprising. R690/R600 and R740/R800 changed only 4–13% with fourfold decreases in photosynthetic rates and twofold decreases in $F_s$ induced by the water stress imposed (Dobrowski *et al.*, 2005). Tools for investigating dynamic photosynthetic changes from remote changes using reflectance and Chl-F are discussed in detail in Chapter 15.

Leaf clipping chl. meters that estimate chl. content rely on leaf transmittances at two red and near infrared wavelengths (Steele *et al.*, 2008).

### 10.2.5. NADPH/NADP: near-ultraviolet absorption and blue fluorescence

Leaves emit BGF when illuminated with UV light. There are two types of information to be obtained from BGF. The first relates to plant phenolic and flavonoid compounds bound to the cell walls or located in vacuoles of epidermal cells (Cerovic *et al.*, 1999). The second concerns the

variation of the concentration and redox state of pyridine nucleotides (NADH and NADPH) and requires very sensitive fluorimeters (Cerovic *et al.*, 1993; Schreiber *et al.*, 1993; review by Cerovic *et al.*, 1999). These cofactors are good BGF fluorophores but, owing to their localisation in mesophyll cells (especially for NADPH in the chloroplasts), they are less accessible to UV excitation and their BGF is re-absorbed by photosynthetic pigments. These facts limit pyridine-nucleotide contribution to BGF in intact leaves to less than 10% in most cases (Cerovic *et al.*, 1993). NADPH-dependent BGF can be changed by applying actinic light to drive photosynthesis (Cerovic *et al.*, 1998).

### 10.2.6. Photoacoustic spectroscopy

Photoacoustic spectroscopy consists in detecting a sound emitted from a light-absorbing material illuminated with a modulated light, usually with a microphone. Light energy at absorbed wavelengths is converted to heat, so that thermal dilatation causes a small volume change that increases and decreases at the frequency of the modulated light oscillations, transmitted to air, thus producing a sound with an intensity proportional to light absorption.

This is called the photothermal effect, which is commonly detected in plant leaves at high modulation frequencies (typically above 100 Hz, reviewed by Malkin and Canaani, 1994). The signal is insensitive to light scattering and depends on absorbed photons, not on transmitted or reflected photons. The fraction of absorbed light energy that is photochemically converted does not produce heat and can be thereby calculated by subtracting the energy converted into heat from the total energy absorbed by antenna pigments. This latter quantity can be measured by adding a strong non-modulated light to the modulated measuring light that will saturate photochemistry and hence will induce maximal energy dissipation in the form of heat. Discrimination between the contributions of the two photosystems can be achieved by using a monochromatic wavelength for excitation. FR light excites mainly PSI, so that changes in the FR-induced photoacoustic signal reflect mainly variations in the activity of PSI. This is particularly useful to follow induction of CEFI (Herbert *et al.*, 1990; Ravenel *et al.*, 1994; Joët *et al.*, 2001) or transitions from state 1 to state 2 corresponding to migration of the peripheral antenna from PSII towards PSI (Veeranjaneyulu *et al.*, 1991; Section 10.3.1).

Photosynthetic material evolves oxygen under light, and the changes of gas volume associated with photosynthetic oxygen formation also produce a sound under modulated light at frequencies below 100 Hz, slow enough to separate the bursts of oxygen (the half-time of oxygen evolution after a flash is ~5 ms). This low-frequency photoacoustic signal specific to oxygenic photosynthesis is called a photobaric signal and reflects gross photosynthesis. The photobaric signal is particularly useful to measure the quantum yield of oxygen evolution or the so-called Emerson enhancement, which gives information on the PSI/PSII activity ratio (Canaani and Malkin, 1984).

## 10.3. CHLOROPHYLL FLUORESCENCE

Chlorophylls in solution emit red/FR fluorescence when excited by photosynthetically active radiations (see Chapter 2, Fig. 2.1). However, the unique property of Chl-F *in vivo* is to be variable, as its yield[2] depends on the functioning of the PSII centre and antenna from which it originates. At the onset of an illumination, the fluorescence yield is minimum ($F_0$) owing to 'photochemical quenching' (qP): energy quanta migrating through the antenna chl.s are trapped to separate a charge pair +/- by 'open' PSII centres, which become temporarily 'closed', i.e., unable to perform another charge separation. The proportion of closed centres increases during illumination and reaches 100% when light is strong enough, corresponding to the maximum fluorescence ($F_m$). The lifetime of excited chl.s, hence their probability to deactivate as fluorescence (Section 10.3.2), is inversely proportional to qP, which varies from one ($F_0$) to zero ($F_m$). The decrease of fluorescence yield following the maximum is ascribable not only to the reoxidation of the primary acceptor $Q_A^-$ by downstream electron transfer, but also to NPQ, a downregulation mechanism that prevents damage as a result of an excess of excited chl.s in the antenna (Section 10.3.4).

The emergence of the modulated fluorescence technique (Schreiber *et al.*, 1986), which allowed the qP and NPQ[3] to be separated, has prompted a great deal of applications in plant physiological and ecophysiological research, as well

[2] Fluorescence yield = fluorescence photons / absorbed photons

[3] Historically, the non-photochemical quenching has been investigated in the early 1980s, using 'light-doubling' intensity instead of saturating pulses.

as in agricultural and environmental monitoring. Many reviews are available (e.g., Govindjee, 1995; book edited by Papageorgiou and Govindjee, 2004; Baker, 2008), including aspects of molecular mechanisms of variable Chl-F emission (Krause and Weis, 1991; Dau, 1994).

### 10.3.1. Fluorescence excitation and emission spectra

Chl. molecules of peripheral and core antennae are bound to proteins, forming complexes with characteristic absorption and fluorescence spectra (see Fig. 2.1). Absorption of one photon, from blue to red, by a chl. molecule produces one singlet excited Chl* storing a quantum of energy corresponding to that of a red photon; this quantum migrates by resonance as an exciton through the antenna, until it is trapped by a photochemical centre or converted into heat or into a red fluorescence photon. Low-temperature (liquid nitrogen: 77K) fluorescence emission spectra of dilute thylakoid suspensions exhibit a sharp band at 685 nm with a shoulder at 695 nm, both corresponding to PSII emission, and a broader band at 730/740 nm, almost absent at ambient temperatures, corresponding mainly to PSI. The two photosystems do not have the same absorption spectra (specifically: more chl. *b* for PSII, chl. *a*–protein complexes absorbing at long wavelengths for PSI), which may result in an imbalance of their photochemical activities, depending on incoming light spectrum. State transition is a corrective mechanism, by which the LHCII connected to the PSII antenna (state 1) becomes phosphorylated when the PQ pool is reduced and then migrates towards the PSI antenna (state 2); this leads to an increase of the 730 nm/685 nm ratio, i.e., PSI/PSII 77K fluorescence emission. Therefore low-temperature fluorescence spectroscopy with photoacoustic spectroscopy (Section 10.2.6) provides a suitable tool to study state transitions. This technique cannot be applied as such to whole leaves, because of the strong reabsorption of the 685/695 nm emission by chl.s, but it works well on a diluted leaf powder obtained by grinding a few $mm^2$ leaf spot with water and quartz particles in liquid nitrogen (Weis, 1985a).

At ambient temperature, the variable Chl-F ($F_v$) in leaves at 685 and 735 nm emanates from PSII (Krause and Weis, 1991), with a 30 to 50% PSI contribution to the $F_0$ fluorescence level in the FR region (Genty *et al.*, 1990; Pfündel, 1998; Agati *et al.*, 2000). PSI has no $F_v$; this is why all the parameters derived from $F_v$ reflect PSII activity. The 685 nm fluorescence is much more re-absorbed by chl.s than 735 nm fluorescence, resulting in a negative curvilinear relation between their ratio and the leaf chl. content. Therefore, F690/F730 ratio is a remote-sensing indicator of leaf chl. content (Lichtenthaler *et al.*, 1990).

### 10.3.2. Lifetime and quantum yield

Picosecond and nanosecond events are the time domains in which chl. emits fluorescence when bound to proteins in the light-harvesting pigment-protein complexes (LHC) of the photosynthetic apparatus. At present, a major limitation for using Chl-F lifetime ($\tau$) for investigation of the photosynthetic process is the complex and expensive electronic system needed for measurements.

A major interest of lifetime measurements in ecophysiology lies in the $\tau/\phi_{PSII}$ relationship. The average lifetime, $\tau$, of excited chl. in the antenna increases when photochemistry slows down, e.g., is inversely proportional to $\phi_{PSII}$, the quantum yield of PSII (Section 10.3.4).

Most of the time-resolved Chl-F measurements reported to date have been carried out in plant materials in which fluorescence has reached a steady state level, including dark-adapted ($F_0$) and illuminated ($F_m$ and $F_s$, in presence and absence of DCMU, respectively) samples (Holzwarth *et al.*, 1985; Moya *et al.*, 1986). Such reports have shown the existence of different (in most cases four) Chl-F components with lifetimes ranging from picoseconds to nanoseconds. The fastest lifetime component ($\tau 1$, 60 ps) is associated with PSI antenna fluorescence (Hodges and Moya, 1986; Agati *et al.*, 2000). $\tau 2$ (270 ps) and $\tau 3$ (550 ps) are components modified by PSII photochemistry and usually associated with PSII (Hodges and Moya, 1986). $\tau 4$ (1.30–3.30 ns) is a minor component associated with free chl. not connected to the functional photosynthetic apparatus.

Chl-F lifetime studies on leaves have been performed mainly under laboratory or greenhouse conditions (Cerovic *et al.*, 1999). $\tau$-LIDAR devices use very short laser pulses (35 ps) and rapid detectors and electronics (streak camera or photomultiplier tube). This permits comparison of the kinetics of emitted Chl-F with the excitation pulse, and allows the average lifetime $\tau$ to be deduced. Also, special fluorimeters have been designed and mounted using time-correlated single-photon-counting detection to resolve the different leaf Chl-F lifetimes (Briantais *et al.*, 1996). One alternative to time-correlated single-photon-counting or direct-decay

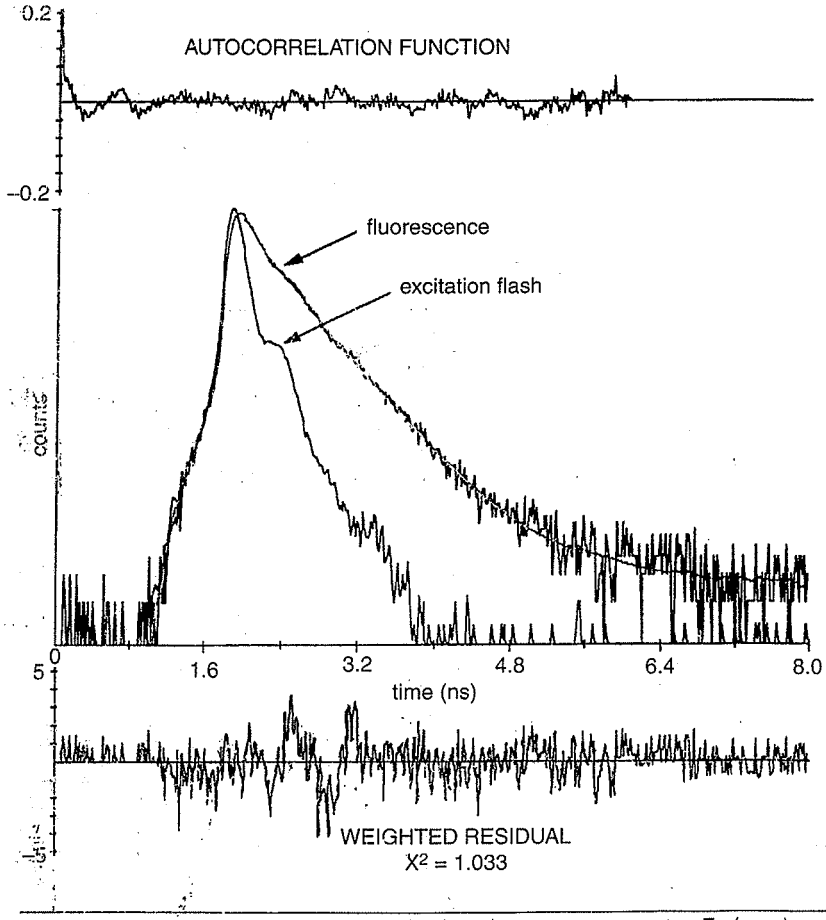


| | +Fe (τ, ns) | -Fe (τ, ns) |
|---|---|---|
| dark-adapted sugar beet leaves | 0.27 ± 0.02 | 0.98 ± 0.20 |
| illuminated sugar beet leaves | 0.43 ± 0.03 | 0.86 ± 0.10 |

Fig. 10.5. Typical chlorophyll-fluorescence (Chl-F) decay and excitation flash from which mean fluorescence lifetime (τ, ns) and their corresponding lifetime components are resolved, using a time-correlated, single-photon counting system (see Morales *et al.*, 2001 for details). Excitation and detection wavelengths were 635 nm and the whole red band of the spectrum, respectively. The figure also shows the mean Chl-F lifetime (τ, ns) in dark-adapted and illuminated sugar beet leaves in plants affected by iron deficiency (control; +Fe, healthy plants; –Fe, Fe-deficient plants). Data are mean±SD. From Morales *et al.* (1999, 2001).

analysis is multifrequency phase modulation fluorimetry, an emerging technique not yet applied in ecophysiology (Moise and Moya, 2004a,b).

There is not much information in the scientific literature on stress-induced changes in Chl-F lifetimes in intact leaves. Increases in Chl-F lifetimes in spruce and pine needles after exposition to high $O_3$ doses (Schneckenburger and Frenz, 1986), heat-stressed barley (Briantais *et al.*, 1996) and in Fe-deficient sugar beet (Morales *et al.*, 1999; Fig. 10.5) and decreases in illuminated, water-stressed leaves (Cerovic *et al.*, 1999) are reported in the literature.

### 10.3.3. The chlorophyll-*a* fluorescence induction (Kautsky effect)

Upon blue illumination of a dark-adapted leaf, Kautsky and Hirsch (1931) observed a red fluorescence emission

of variable intensity, which first rose to a maximum then decayed more slowly. This constitutes the fluorescence induction (now called OJIP): at the onset of a constant illumination, the fluorescence yield starts increasing from a minimum level O ($F_0$: constant fluorescence) to reach, within hundreds of milliseconds, a maximum level P ($F_p$). P grows with excitation intensity until it saturates between 300 and 1000 µmol $m^{-2}$ $s^{-1}$ depending on light spectrum and plant material, to an absolute maximum level $F_m$ (Fig. 10.6A). The fluorescence rise reflects the reduction of the primary acceptor $Q_A$ (open centre) to $Q_A^-$ (closed centre). The increase of the fluorescence yield under light corresponds to a build-up of the high fluorescence $P680Q_A^-$ state of PSII centres, resulting from the fast re-reduction of $P680^+$ by the primary donor Tyr-Z (see Section 10.2.2, also Chapter 2). Closed PSII centre are unable to trap another incoming light quantum, which stays longer in the antenna with a higher probability to deactivate by emitting a fluorescence photon (Section 10.3.2). The difference $F_v=F_m-F_0$ is the variable fluorescence. A ratio $F_v/F_m=0.84$ has been measured in several angiosperm species (Björkman and Demmig, 1987). In practice, a value of ~0.8, obtained under a saturating light pulse after dark adaptation in leaves, where emission around 730 nm is prominent (cf Section 10.3.2), indicates a fully efficient PSII. The shape of the fluorescence rise from $F_0$ to $F_m$ depends on the excitation intensity (Fig. 10.6A). It appears biphasic at moderate light intensities (<1000 µmol $m^{-2}$ $s^{-1}$), and triphasic at high light intensities in intact organisms and leaves (>1000 µmol $m^{-2}$ $s^{-1}$), with two intermediate levels originally called $I_1$ and $I_2$ (Neubauer and Schreiber, 1987; Schreiber and Neubauer, 1987), and subsequently J and I (Strasser *et al.*, 1995). The fluorescence intensity decreases after P, exhibiting several characteristic points S, M and T that can be observed especially at moderate light intensities (Papageorgiou *et al.*, 2007).

Freezing the sample in liquid nitrogen or infiltrating it with DCMU to block the electron transfer from $Q_A$ to $Q_B$ converts the bi- or triphasic kinetics into a single photochemical rise reflecting the reduction of the primary quinone acceptor $Q_A$ (see Chapter 2). The complementary area (area of rectangle with $F_0$ and $F_m$ opposite corners *minus* area under the rise curve) is a measure of the pool of electron acceptors of PSII: this area without DCMU is 10 to 15-fold that with DCMU, consistent with the $PQ/Q_A$ ratio, i.e., the number of PQ molecules per PSII centre.

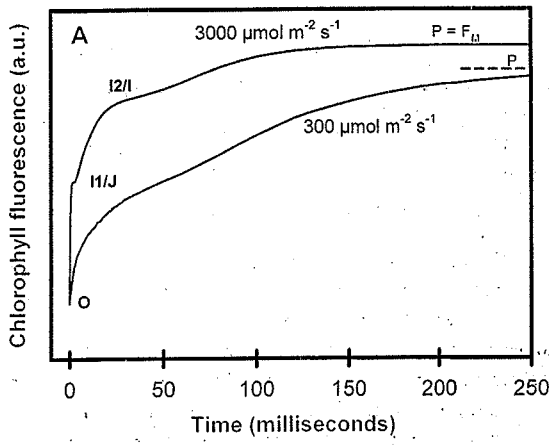


Fig. 10.6. Fluorescence induction and variation of its determining parameters. (**A**) Chlorophyll-fluorescence (Chl-F) induction transients recorded during 1 second on pea leaves, normalised to $F_0$. Excitation by 300 and 3000 µmoles $m^{-2}$ $s^{-1}$ continuous red light (650 nm peak wavelength). Fluorescence emission measured above 700 nm. The first reliably measured point of the fluorescence transient is at 20 µs, taken as $F_0$. Handy PEA instrument (Hansatech Instruments Ltd, UK). Maximum P for lower curve is at 800 ms. Credit S.Z. Toth. (**B**) Fluorescence induction kinetics. (**C to E**): Schematic representations of key factors causing the fluorescence variation shown in panel (**B**). The fluorescence trace in (**B**) was recorded with a dark-acclimated leaf. First, in the dark, minimum fluorescence ($F_0$) was established (conditions: PSII reaction centres closed, low trans-thylakoid pH gradient (ΔpH), and low zeaxanthin content), see (**C to E**). Also in the dark-acclimated state, a strong but relatively short (0.6 s) saturating pulse (SP) was applied to close PSII reaction centres transiently and, thus, to increase fluorescence to the maximum level, $F_m$. Thereafter, 180 s of actinic light was given (*cf.* 'ACTINIC LIGHT' on top of figure): during illumination variations in the closure state of PSII reaction centres (**C**), ΔpH (**D**) and zeaxanthin (**E**) occurred, which produced a typical Kautsky type fluorescence induction kinetics. At the end of illumination, the maximum fluorescence level ($F_m'$) was elicited by an SP. Immediately thereafter, actinic light was switched off and the minimal fluorescence in the light-acclimated state ($F_0'$) was assessed during post-pulse exposure to far red light: the FR predominantly drives PSI with the effect that electrons are withdrawn from the inter system electron chain and that PSII reaction centres become fully open while the factors involved in non-photochemical fluorescence quenching (ΔpH and zeaxanthin) are still active. Source of panels B to E: E. Pfündel, JUNIOR-PAM Handbook of operation, Walz; with permission.

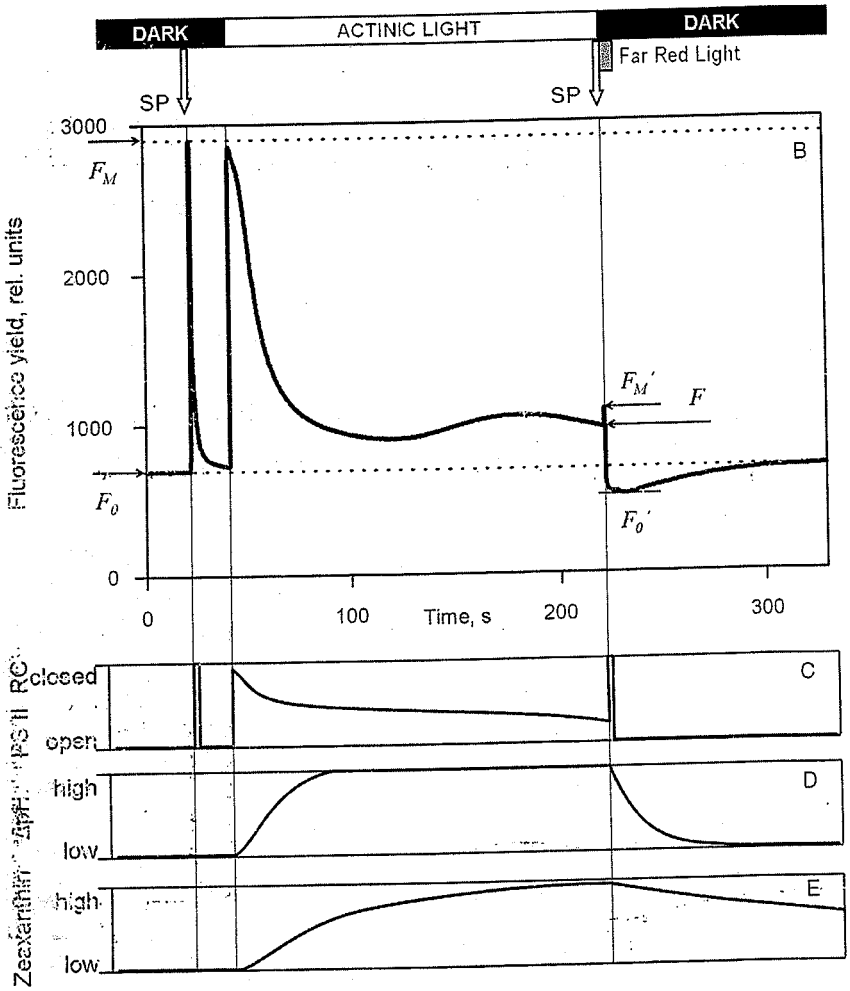


Fig 10.6. (*cont.*)

The $I_1$(J) level (also called step) unambiguously corresponds to that previously called I[+] (Delosme, 1967) and reflects the reoxidation of $Q_A^-$ by the PQ pool. The half-time of the photochemical O → $I_1$ phase progressively shifts from tens of milliseconds to hundreds of microseconds when excitation intensity is increased. Consistently, $I_1$(J) is specifically increased by low concentrations of DCMU that binds to the $Q_B$ site or by the triazine-resistance mutation Ser264Gly in the $Q_B$ site (Hiraki *et al.*, 2003) that slows down the $Q_A^-$ → $Q_B$ transfer.

The $I_2$(I) level at about 30 ms appears under light intensities above 1000 μmol $m^{-2}$ $s^{-1}$ in dark-adapted leaves. The $I_2$(I) → P phase corresponds to the reduction of the pool of electron acceptors of PSI (Schansker *et al.*, 2005). $I_2$(I) vanishes in pre-illuminated leaves, because the Calvin cycle activated by light reoxidises the PSI acceptors and in disrupted chloroplasts as a result of the loss of Fd.

A new step K exhibiting a maximum at 300–400 μs (Guissé *et al.*, 1995; Tóth *et al.*, 2007) substitutes the $I_1$(J) step when the oxygen-evolving complex (OEC) is damaged, for example by heat treatment.

A proper tuning of excitation light intensity is important to get appropriate responses from OJIP kinetics. Intensities between 200 and 1000 μmol $m^{-2}$ $s^{-1}$ raise the P level close

[+] It should be noticed that the *I* level in the classical Chl-F literature corresponds to *J* not *I* in the newer OJIP nomenclature.

to $F_m$ while keeping the $I_1$(J) level low; these conditions are optimal to detect an inhibition at the acceptor side of PSII and to monitor the penetration, migration and detoxication of DCMU-like herbicides in plants (Ducruet *et al.*, 1984; Habash *et al.*, 1985). Higher light intensities reveal the two $I_1$(J) and $I_2$(I) levels, with a shape depending on plant species (Tyystjärvi *et al.*, 1999).

The $Q_A^-$ to $Q_B$ and $Q_A^-$ to $Q_B^-$ electron-transfer steps can be directly investigated after a few microseconds saturating flash that forms $Q_A^-$, corresponding to a high fluorescence-state yield. The decay of fluorescence yield detected by a weak analytical excitation reflects the reoxidation of $Q_A^-$, with a main phase in the hundreds of microseconds range (Bowes and Croft, 1980).

### 10.3.4. Modulated fluorescence and quenching analysis

The technique of pulse amplitude modulation (PAM) emerged in the mid-1980s (Schreiber *et al.*, 1986) and made it possible to measure fluorescence yield by a modulated analytical excitation during a continuous actinic illumination. LED pulses of variable frequency[5] constitute the measuring (analytical) light: the small fluorescence surges corresponding to light pulses appear superimposed on background emission and provide a measure for the fluorescence yield. Saturating light pulses lasting a few hundreds of milliseconds, also called flashes, reveal two types of fluorescence quenching, qP and NPQ (Schreiber *et al.*, 1986). This technique allowed the actual PSII efficiency ($\phi_{PSII}$) of illuminated leaves to be estimated (Genty *et al.*, 1989). Measurements are done with a portable or laboratory PAM-type fluorimeter and involve two successive measurements on the same leaf (Fig. 10.6B). First, fluorescence is measured after dark adaptation to obtain the $F_0$ and $F_m$ fluorescence levels (corresponding to open $Q_A$ and closed $Q_A^-$ centres, respectively, as defined above). Later on, modulated Chl-F is measured under continuous illumination until the stationary state ($F_s$) is attained. During continuous illumination, saturating light pulses (400 to 1200 ms) are applied to establish $F_m'$, lower than the dark-measured $F_m$ owing to NPQ. After turning out the actinic light, a short interval of FR light can be used to obtain the $F_0'$ fluorescence level. $\phi_{PSII}$ is calculated as the quotient $(F_m'-F)/F_m'$. $\phi_{PSII}$ depends on two factors: (1) the proportion of open, oxidised PSII *RC*s (estimated by the so-called photochemical quenching, qP, calculated as quotient $(F_m'-F)/F_v'$, where $F_v'$ is $F_m'-F_0'$); and (2) the intrinsic PSII efficiency that is estimated by the $F'_v/F'_m$ ratio. $\phi_{PSII}$ is therefore equal to qP x $F'_v/F'_m$ (Genty *et al.*, 1989). Under high light intensities, such as those encountered in field conditions, the light pulse may not be strong enough to close all PSII *RC*s in order to reveal the real $F_m'$ level. This problem can be solved by using successive non-saturating pulses (Markgraf and Berry, 1990; Earl and Ennahli, 2004) or a multiphase single pulse (Loriaux *et al.*, 2006) with decreasing intensities, then extrapolating these apparent $F_m'$ values to infinite light intensity to determine $F_m'$ exactly.

The access to $\phi_{PSII}$ allows the electron-transfer rate through PSII ($\mathcal{J}_f$) to be calculated, a major application of modulated Chl-F (Genty *et al.*, 1989). The $\mathcal{J}_f$ is defined as $\varphi_{PSII}\times PPFD\times\alpha_L\times\varepsilon_{PSII}$ where PPFD is the PAR photon-flux density; $\alpha_L$ is the fraction of incoming PAR that is absorbed (not transmitted nor reflected); and $\varepsilon_{PSII}$ is the fraction of these quanta absorbed by PSII, $1-\varepsilon_{PSII}$ by PSI. In a first approximation, it can be considered that $\alpha_L$=0.85 and $\varepsilon_{PSII}$=0.5. The product $\alpha_L\times\varepsilon_{PSII}$ can be more accurately determined (Valentini *et al.*, 1995a) from the relationship between $\phi_{PSII}$ and $\phi_{CO2}$ obtained by varying light intensity in an atmosphere containing 1% $O_2$ in order to eliminate photorespiration. The possibility to measure $\mathcal{J}$ through PSII by fluorescence allowed, for example, to demonstrate that $\mathcal{J}_f$ was much less reduced by moderate drought than the assimilation of $CO_2$ inhibited by stomatal closure, the electrons being routed towards photorespiration (Cornic and Briantais, 1991).

NPQ, the rate constant of thermal deactivation, can also be estimated from modulated Chl-F data ($(F_m/F_m')-1$). A major component of NPQ is the electrochemical quenching qE that depends both on an acidic lumen ($\Delta$pH) and of conversion of violaxanthin to zeaxanthin (Fig. 10.6B); it relaxes within a few minutes in the dark. qT as a result of state transitions (Section 10.3.1) and qI as a result of photoinhibition have longer dark relaxation times. NPQ is reduced by uncoupling or stress-induced membrane leakiness; it is increased when a strong proton gradient builds up upon triggering of CEFI (Makino

[5] Analytical or unactinic excitation = measuring light with an intensity low enough not to influence the observed phenomenon. An LED pulsed at a low frequency (e.g., 9 kHz), not actinic in darkness owing to the very low average light intensity, is used to measure $F_0$, but it can be set at a higher frequency (e.g., 100 kHz) under illumination to improve the signal-to-noise ratio.

*et al.*, 2002). Applications of modulated fluorescence to leaf photosynthesis have led to thousands of published works, especially concerning stress physiology, which cannot be briefly summarised here (see book edited by Papageorgiou and Govindjee, 2004; reviews by Baker, 2008; and those cited in Chapters 16 and 21). Improvements and possible pitfalls in particular conditions are still being discussed (e.g., see Buckley and Farquhar, 2004; Peguero-Pina *et al.*, 2009).

### 10.3.5. Thermofluorescence: $F_0$, $F_m$ during warming or freezing

Under a very weak exciting light, the rate of closure of PSII traps by incoming photons is slower than their reopening by downstream electron transfer or charge recombination, so that this fluorescence level stays minimum ($F_0$)[6]. At temperatures above 40°C however, $F_0$ progressively increases. This can be optimally resolved during a slow warming (e.g., 1°C/min) in the form of $F_0$ versus temperature ($F_0$/T) curves (Schreiber and Berry, 1977; Berry and Björkmann, 1980; Briantais *et al.*, 1996) that exhibit a maximum emission at about 55–60°C followed by a shoulder, or sometimes a second maximum near 70°C. The intersection of the tangent to the fluorescence rise with the horizontal initial $F_0$ level defines a characteristic temperature Tc, between 40 and 50°C, correlated with the heat sensitivity of leaves measured afterwards by leaf necrosis (Bilger *et al.*, 1984). The fluorescence $F_m$ level starts decreasing with temperature above 30°C, so that the $F_m$/T curve meets the $F_0$/T curve at its maximum near 60°C.

$F_0$/T curves are a tool to characterise the thermal sensitivity of PSII in leaves, which depends on the thermal adaptation of plant species and on previous heat acclimation (Bilger *et al.*, 1984; Terzaghi *et al.*, 1989). They are shifted towards higher temperature by illumination or drought (Havaux, 1992; Rekika *et al.*, 1997; review by Ducruet *et al.*, 2007). An acidic pH in the lumen or non-electrolytes solutes such as sugars protect PSII from heat damage (Williams *et al.*, 1992).

A temperature-dependent increase of $F_0$ and decrease of $F_m$ is also observed in leaves during slow freezing (Sundbom *et al.*, 1982; Pospisil *et al.*, 1998; Neuner and Pramsohler, 2006), corresponding to the nucleation temperature at which water in a supercooled state almost instantly crystallises with a temperature burst detectable by IR thermography.

## 10.4. CHLOROPHYLL LUMINESCENCE (DELAYED FLUORESCENCE)

In leaves previously illuminated, a faint glow of red light decaying within minutes can be recorded in darkness with sensitive detectors. Its emission spectrum is similar to that of chl. 'prompt' fluorescence emitted during light excitation. This dark emission is indeed a 'delayed' fluorescence, called luminescence for clarity, and also originates from PSII. Luminescence results from the recreation, with a low yield, of an excited singlet chl. by the recombination of a +/- charge pair previously separated by the photochemical conversion of a light quantum. The positive charges are stabilised on the S states of the OEC ($S_{2(+)}$, $S_{3(+)}$, storing two or three positive charges on a manganese complex) of PSII while an electron is usually stored on the secondary quinone acceptor $Q_B^-$ (Chapter 2). Each type of charge pair produces a characteristic luminescence decay phase or a thermoluminescence (TL) band. While prompt fluorescence depends on the state of PSII antenna and centre, delayed fluorescence or luminescence depends on the charge distribution on PSII electron carriers beyond the photochemical tarp. This distribution can be controlled by using 'single turnover' flashes (STOF) powerful and short enough to induce only one charge separation in every centre[7].

### 10.4.1. Luminescence-decay kinetics

Luminescence-decay kinetics can be recorded easily after illumination of a leaf piece maintained at a constant temperature in a dark room or box, simply by opening a shutter that protects the detector (usually a photomultiplier) during illumination. Temperature control is essential because

[6] $F_0$ can be measured either by a modulated fluorimeter operated at low frequency or by coupling an ultra-low blue exciting light to a sensitive fluorescence detection (photomutiplier) behind a red filter.

[7] This can be achieved using xenon bulbs that deliver a few microsecond flashes. They emit, however, a weak long-lasting glow or tail that interfers with low-level luminescence measurements in the millisecond range, making a flash shutter necessary. LEDs have become powerful enough to produce saturating square light pulses shorter than 10 µs without tail. The STOF flashes are different from the saturating flashes used for modulated fluorescence, that last for hundreds of milliseconds. For controversial reasons, $F_m$ cannot be reached upon one STOF.

Table 10.2. *Origin of thermoluminescence bands. $T_M$ values correspond to a 0.5°C/s thermoluminescence heating rate.*

| Name | $T_m$ range | Origin | PSII | Comments |
|---|---|---|---|---|
| $A_T$ | –10 to –20°C | TyrZ + $Q_A^-$ | + | Damage to Mn oxygen-evolving complex (TyrZ is the functional donor to PSII center) |
| A | ~ –15°C | $S_3Q_A^-$ ? | + | — |
| Q | +2 to 10°C | $S_2Q_A^-$ | + | Damage to secondary $Q_B$ quinonic acceptor or inhibition by DCMU-like herbicides |
| B | 30 to 38°C | $S_{2/3}Q_B^-$ | + | Lumen pH neutral |
| B2 | 28 to 32°C | $S_2Q_B^-$ | + | Lumen pH slightly acidic |
| B1 | 20 to 30°C | $S_3Q_B^-$ | + | " " |
| AG | +45°C (→+35°C) | $S_2/S_3Q_B + e^-$ | (+) | $e^-$ from stroma, in intact chloroplasts or cells |
| C | +52/55°C | TyrD + $Q_A^-$ | + | Minor band, increased by DCMU or damage (TyrD is the non-functional donor to PSII centre) |
| HTL1 | 60 to 85°C | ? | — | Different bands of unknown origin |
| HTL2 | 120 to 40°C | Lipid peroxides | — | Thermolysis: -C-O-O- → *C=O + Chl → *Chl |

of the high-temperature dependence of luminescence emission. Recording decay phases faster than 0.1 s requires special technical precautions (Section 10.4.3).

Luminescence decays can be theoretically decomposed into exponentials, corresponding to TL bands (Section 10.4.2). Practically this proves unreliable in leaves owing to the occurrence of non-exponential decay phases. Therefore TL is often preferred for its better resolving capacity, even though DL as a non-destructive technique may be needed for example when periodical measurements have to be done on the same leaf or for non-contact sensing in darkness.

### 10.4.2. Thermoluminescence

The +/– charge pairs produced by illumination are stabilised in energetic wells, with 'activation-energy' barriers limiting the back reaction, which makes photosynthesis possible. Increasing temperature, i.e., vibrational energy, enhances the recombination over these barriers according to the Arrhenius equation. TL is a technique that consists of illuminating the sample at a temperature cold enough to practically block the recombination of the investigated charge pairs and to reveal them by a progressive warming (0.1 to 0.6°C/s) as successive TL bands (see Table 10.2) peaking at increasing temperatures (reviews by Vass and Govindjee, 1996; Ducruet, 2003; Gilbert *et al.*, 2004; Tyystjärvi and Vass, 2004). These bands often overlap and can be separated by fitting elementary components governed by three parameters (activation energy $E_A'$; pre-exponential factor; area, from which the peak temperature Tm can be derived) calculated by analytical or numerical methods (Vass *et al.*, 1981; Ducruet, 2003).

In a healthy photosynthetic organism, PSII charge pairs +/- are stabilised as $S_2Q_B^-$ and $S_3Q_B^-$ states able to recombine with luminescence emission, corresponding to one or two B bands observed in the 20 to 38°C temperature range (Rutherford *et al.*, 1982, 1984; see Chapter 2). The intensity of the B band oscillates with a period 4 according to the number of flashes, reflecting the four-step turnover of S state of the OEC. The B band often splits into a $B_1$ band (~20–25°C) corresponding to $S_3Q_B^-$ and a $B_2$ band (~30°C) to $S_2Q_B^-$. This split can be explained by a greater proton uptake (Lavergne and Junge, 1992) in $S_3Q_B^-$ than in $S_2Q_B^-$ recombination steps. The temperature downshift of the $S_3Q_B^-$ band induced by two or three flashes is a direct probe of the dark-stable pH of lumen in unfrozen leaves.

Destruction of PSII under stress conditions results in a decrease of the B-band(s) intensity along with the $F_v/F_m$ fluorescence ratio, and may be accompanied by the enhancement of minor bands. The Q band at ~5°C, produced by the inhibitor DCMU that blocks the $Q_B$ pocket, corresponds to $S_2Q_A^-$ and indicates damage to the PSII acceptor side. Bands A/At (–20°C) reflects damage to PSII OEC.

A major requirement for using (thermo)luminescence for *in vivo* photosynthesis studies is to prevent freezing below the nucleation temperature (~–5°C), under which ice crystals break thylakoid membranes. This dissipates

the proton and ionic gradients and in some species grossly distorts the signal (Homann, 1999; Janda *et al.*, 2004).

An 'afterglow' emission (AG) can be observed in unfrozen leaves, algal cells or intact chloroplasts, appearing as a delayed luminescence burst superimposed to luminescence decays (Bertsch and Azzi, 1965), or as a sharp TL band at about 45°C (Fig. 10.7). It is generally induced by FR light, or sometimes by flashes or white light pulses depending on plant species and growth conditions. It originates from the PSII 'silent'centres $S_2Q_B$ and $S_3Q_B$, unable to emit luminescence; these centres become enabled to undergo +/- charge recombination and hence to emit luminescence when an electron is back-transferred to $Q_B$ (Sundblad *et al.*, 1988). Electrons follow the cyclic/chlororespiratory pathway(s) connecting the pool of reductive compounds stored in the stroma to electron carriers of the intersystem chain. Temperatures above 30°C stimulate this pathway (Weis, 1985b; Havaux, 1996). Consistently the afterglow emission (AG) is enhanced by warming and can be optimally resolved as a sharp TL band peaking at 45°C with a 0.5°C/s warming rate (Miranda and Ducruet, 1995). Cyclic/chlororespiratory pathways can be induced at ambient temperatures by stress treatments (e.g., high light, anoxia, cold, drought). For example, anoxia induces CEFI (Joët *et al.*, 2002) and thereby allows the electron transfer from stroma to $Q_B$ to occur at lower temperatures, resulting in a temperature downshift of the AG band that ultimately fuses with the B band (Fig. 10.7A). This downshift of AG is correlated to a faster re-reduction of $P700^+$ after a FR-light excitation (Ducruet *et al.*, 2005; Apostol *et al.*, 2006) that also characterises an opening of cyclic pathways in the dark (Section 10.2.2).

The variations of the $NADPH^+ATP$ assimilatory potential, in equilibrium with the pool of ATP in the stroma (Gerst *et al.*, 1994), determine those of AG intensity (Krieger *et al.*, 1998). Its increase reflects a slower $CO_2$ fixation in case of, for example, low $CO_2$ in algae (Palmqvist *et al.*, 1986), induction of CAM metabolism (Krieger *et al.*, 1998), viral infection (Sajnani *et al.*, 2007) and drought (Fig. 10.7B).

Chl-F and (thermo)luminescence both originate from PSII, but provide complementary information on a wider range of the photosynthetic metabolism.

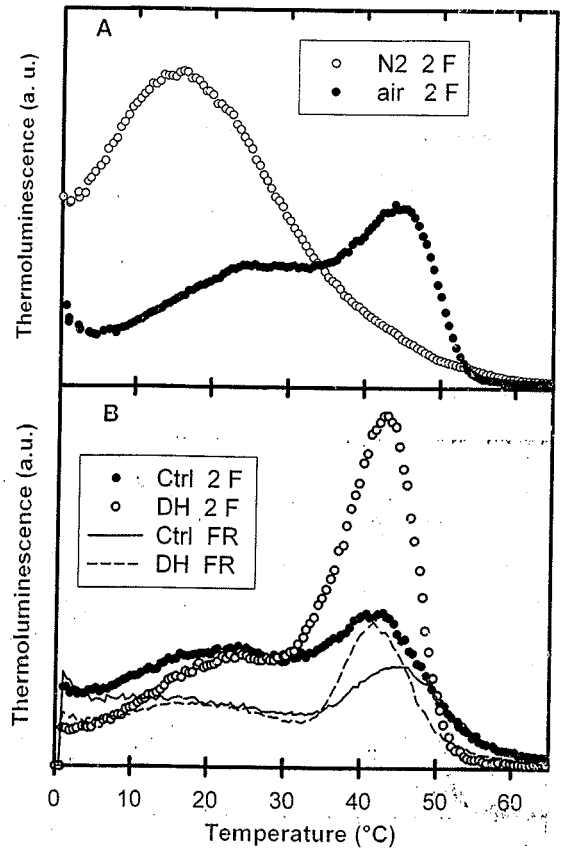


Fig. 10.7. Induction of cyclic pathway(s) by anoxia and increase of NADPH+ATP potential by drought, monitored by the afterglow thermoluminescence band. (A) Effect of anoxia (2 min nitrogen gas) on pea. Paired leaflets, 1-hour dark adapted. Control in air shows a B band as a shoulder at 25°C and an AG band at 46°C. Anoxia causes the AG to fuse with the B band, with a downshift of B caused by a lower lumen pH. (B) Effect of drought on barley leaves. Plants watered (ctrl) or not (drought, DH) after 6 days (8-hours dark adaptation). The AG band at ~40°C induced by two flashes (2F) is increased by drought, reflecting a higher NADPH+ATP potential that is not dissipated by the Calvin cycle owing to stomatal closure. The AG band induced both by two flashes or 10 s FR is downshifted by ~5°C, indicating a slight induction of cyclic pathway(s) (corresponding to faster re-reduction of P700 after FR, not shown). The $S_2/S_3$ luminescence emitting states of OEC are 100% of PSII centres after two flashes, 50% after FR. (V. Peeva *et al.*, unpublished).

### 10.4.3. Fast luminescence decay and modulated luminescence (DLE)

Fast luminescence-decay phases exist in the millisecond and submillisecond time domain. Historically, a so-called delayed light emission was measured under a steady state periodical excitation using a rotating-disc phosphoroscope. The availability of light emitting diodes (LED) brought more flexibility and allowed fluorescence OJIP rise and

luminescence decay to be recorded on an LED pulse. Several luminescence-decay phases in the millisecond and microsecond time range (Zankel, 1973) offer insight into the early steps of oxygen evolution. A phase recorded in the 0.5- to 5-ms time interval (Boussac *et al.*, 1985) has proved useful to follow the building up of the ΔpH under light. It occurs after three single turnover flashes that produce the putative transient state $S_4$, more exactly $Z + S_3$, leading to $O_2$ evolution within ~5 ms after the last flash:

$$S_3 + h\nu \leftrightarrow S_3 + Z^+ + n\,H^+ \rightarrow S_4 \rightarrow S_0 + O_2 \quad \text{[Eqn. 10.2]}$$

with n=1.5 to 2 protons taken up during the reverse luminescence-emitting step (Lavergne and Junge, 1992). This makes the 5-ms luminescence decay from $S_3Z^+$ a good sensor of lumen pH. It is possible to record stroboscopically both a fluorescence rise during the illumination periods and a luminescence rise during the dark periods (Malkin *et al.*, 1994), the latter reflecting the light-driven 'energisation' of thylakoids (e.g., building up of the *pmf*, see Section 10.2.3). Steady state modulated luminescence (DLE) recorded at increasing temperatures shows a maximum near 15°C in chilling-sensitive species only, and another one around 40°C: both indicate an increased membrane leakiness as a result of fluid ↔ gel phase transitions of saturated membrane lipids and temperature-induced membrane disorder, respectively (Havaux and Lannoye, 1983; Fork *et al.*, 1985; Fork and Murata, 1990; review by Ducruet *et al.*, 2007). DLE sensing of the transmembrane electrical field ΔΨ and proton gradient ΔpH is related to that performed by green-light-absorption methods (Section 10.2.3) and to fluorescence NPQ (Section 10.3.4).

### 10.4.4. High-temperature thermoluminescence and oxidative stress

Heat damage to PSII starts at ~40°C, with full destruction above 60°C (Section 10.3.5). Nevertheless, TL bands can be observed at higher temperature without prior illumination as a heat-induced chemiluminescence (Vavilin *et al.*, 1991; Vavilin and Ducruet, 1998; Havaux and Niyogi, 1999; review by Havaux, 2003). This emission results from a radiative thermolysis of peroxide-containing -O-O-C- bonds that generate excited carbonyls, which subsequently excites red Chl-F in leaves or blue or green direct-light emission (Abeles, 1986). This high-temperature thermoluminescence (HTL) exhibits a main band close to 130°C (HTL2), its area being correlated with the amount of peroxides measured by chemical techniques (reaction with thio-barbituric acid, ethane evolution). The leaf sample should be allowed to dry during warming to prevent non-radiative hydrolysis that increases with temperature and competes with the luminescence-emitting radiolysis. This chemiluminescence stimulated by warming also occurs at ambient temperature as an ultra-weak luminescence, detectable by highly sensitive, albeit costly, photomultipliers or cameras (Abeles, 1984; Flor-Henry *et al.*, 2004; Havaux *et al.*, 2006). The HTL and ultra-weak luminescence can be used for imaging oxidative stress in leaves (Section 10.6).

## 10.5. EXPERIMENTAL ASPECTS OF OPTICAL MEASUREMENTS ON LEAVES

### 10.5.1. Summary of other optical methods not related to photosynthesis

Chl. can be used as an internal probe to estimate the epidermal transmittance from the ratio of Chl-F yields induced by UV and blue-, green- or red-excitation lights (Bilger *et al.*, 1997; Ounis *et al.*, 2001a; Pfündel *et al.*, 2007) either in leaves or fruits (Cerovic *et al.*, 2002; Kolb *et al.*, 2003; Agati *et al.*, 2007).

Leaves fluoresce not only red light from chl., but also blue-green light from polyphenolic compounds (Lichtenthaler and Miehé, 1997; Cerovic *et al.*, 1999) when illuminated with UV light or blue light (Sections 10.2.5 and 10.6).

Assessing optically the content of various polyphenols in epidermis is in growing use in agriculture, e.g., for optimising nitrogen fertilisation of crops, early detection of pathogen infection (see Chapter 22) and detection of fruit ripeness.

Infrared thermometry allows to measure leaf temperature remotely and monitor its increase by closure of stomata and decreased transpiration. It can be combined with photosynthetic optical measurements, such as Chl-F (Chaerle *et al.*, 2006, Section 10.6) or visible and NIR spectroscopy, especially in remote sensing.

### 10.5.2. Instruments: optronics for optical measurements

Applications of optical methods outside biophysical laboratories have been hindered by the lack of user-friendly, (trans)portable and affordable instruments. Tremendous advances in optronics during the last 25 years and emergence of a wider market for agricultural and environmental monitoring have both favoured the development of commercial instruments.

LED and laser diodes that can be easily modulated now cover the whole PAR spectrum, from IR to UV, and have become powerful enough to replace lamps and xenon flashes. In addition to now widely used solid-state silicon photodiodes (PIN) more sensitive avalanche photodiodes (APD) and pocket-size photomultiplier modules with integrated power supplies and amplifiers are available for weak signals (luminescence, phytoplankton fluorescence, remote sensing). The temperature control of samples has been greatly simplified and made flexible by solid-state 'Peltier' thermoelectric elements. Computer interfaces allowing both signal recording and instrument driving with real-time signal analysis have played a major role in the diffusion of optical techniques outside laboratories.

In a similar way to medical indicators (stethoscope, thermometer, etc), several optical indicators are necessary to diagnose correctly the physiological status of vegetation. Complementary measurements on the same leaf spot, using mutifurcated fiber optics or inserting various LEDs and detectors in a compact measuring head, rules out the variability between leaf samples especially in wild species.

Beyond ecophysiological research, optical methods are expanding in environmental survey, precision farming and genetic phenotyping: for these applications proximal non-contact sensing is often preferred to more time-consuming and somewhat tricky leaf clipping.

## 10.6. IMAGING TECHNIQUES FOR PLANT-STRESS DETECTION

Measurement of Chl-F from leaves reveals basic information about the component processes in the light reactions of photosynthesis, and non-imaging chl. *a* fluorometry has been recognised as a non-invasive, highly sensitive probe of the responses of photosynthetic processes to stress (see the book *Chl a Fluorescence: A Signature of Photosynthesis*, Papageorgiou and Govindjee (eds), 2004). However, single-point measurements are not representative for a whole sample, and only imaging provides the information about photosynthetic and metabolic gradients (induced by stress or plant development) of different fluorescence signals over a sample (Lichtenthaler *et al.*, 2005). Visualisation of the light signals emitted by a plant can track the movement of herbicides (Fig. 10.8) or the spreading of a pathogen through its host (Chaerle *et al.*, 2006; Pérez-Bueno *et al.*, 2006; Pineda *et al.*, 2008a,b). The limitations of conventional spectrofluorometers, recording Chl-F and BGF emission spectra or gas-exchange devices measuring stomatal conductance and $CO_2$ assimilation in very small areas, could be overcome by multispectral fluorescence or thermal imaging. In the last two decades, new *in vivo* imaging approaches (Jones and Morison, 2007) from the subcellular to the ecophysiological level have been developed to study different plant processes and their modulation by the environment. The future is a multisensor approach where a combination of at least reflectance, fluorescence and thermal imaging will facilitate basic research, field screening and stress diagnosis in the frame of a precision agriculture with a lower environmental impact.

### 10.6.1. Chlorophyll-fluorescence imaging

Techniques allowing the visualisation of the spatial distribution of fluorescence have been implemented both in laboratories as well as in field experiments. Fluorescence can be captured from individual chloroplast, single cells, microalgae, plant organs, whole plants or canopies, and can be applied from the microscopic to the remote-sensing scale (Daley, 1995; Nilsson, 1995; Baker *et al.*, 2001; Chaerle and Van Der Straeten, 2001; Nedbal and Whitmarsh, 2004; Aldea *et al.*, 2006a; Baker, 2008). FI is becoming a promising tool to be used in screening programmes for crop-yield management (Baker and Rosenqvist, 2004). It is applied for mutant screening, analysis of fruit quality and post-harvest damage, study of secondary metabolism, visualisation of source-sink relationships and monitoring of abiotic stress factors including herbicides, wounding, oxidative stress, ozone, nutrient deficiencies and others. The Chl-FI tool is especially valuable in the case of biotic stress where non-uniform alterations of photosynthetic activity and symptom development is expected (Section 22.8 of this book is devoted to imaging methods for biotic stress detection).

The technology and methodology to image Chl-F and obtain the spatial pattern of a range of fluorescence parameters are reviewed in Nedbal and Whitmarsh (2004) and Oxborough (2004). Commercial Chl-F instruments are available (Table 10.1). A number of Chl-FI instruments have been developed by different research groups for research at the microscopic level (Oxborough and Baker, 1997; Osmond *et al.*, 1999; Holub *et al.*, 2000; Küpper *et al.*, 2000; Rolfe and Scholes, 2002; reviewed in Oxborough, 2004) or at low resolution (Omasa *et al.*, 1987; Daley *et al.*, 1989; Fenton and Crofts, 1990; Genty and Meyer, 1995; Siebke and Weiss, 1995; Scholes and Rolfe, 1996; Osmond *et al.*, 1998; Nedbal *et al.*, 2000b; Chaerle and van der Straeten, 2001; Zangerl *et al.*, 2002; Valcke, 2003; Oxborough, 2004).

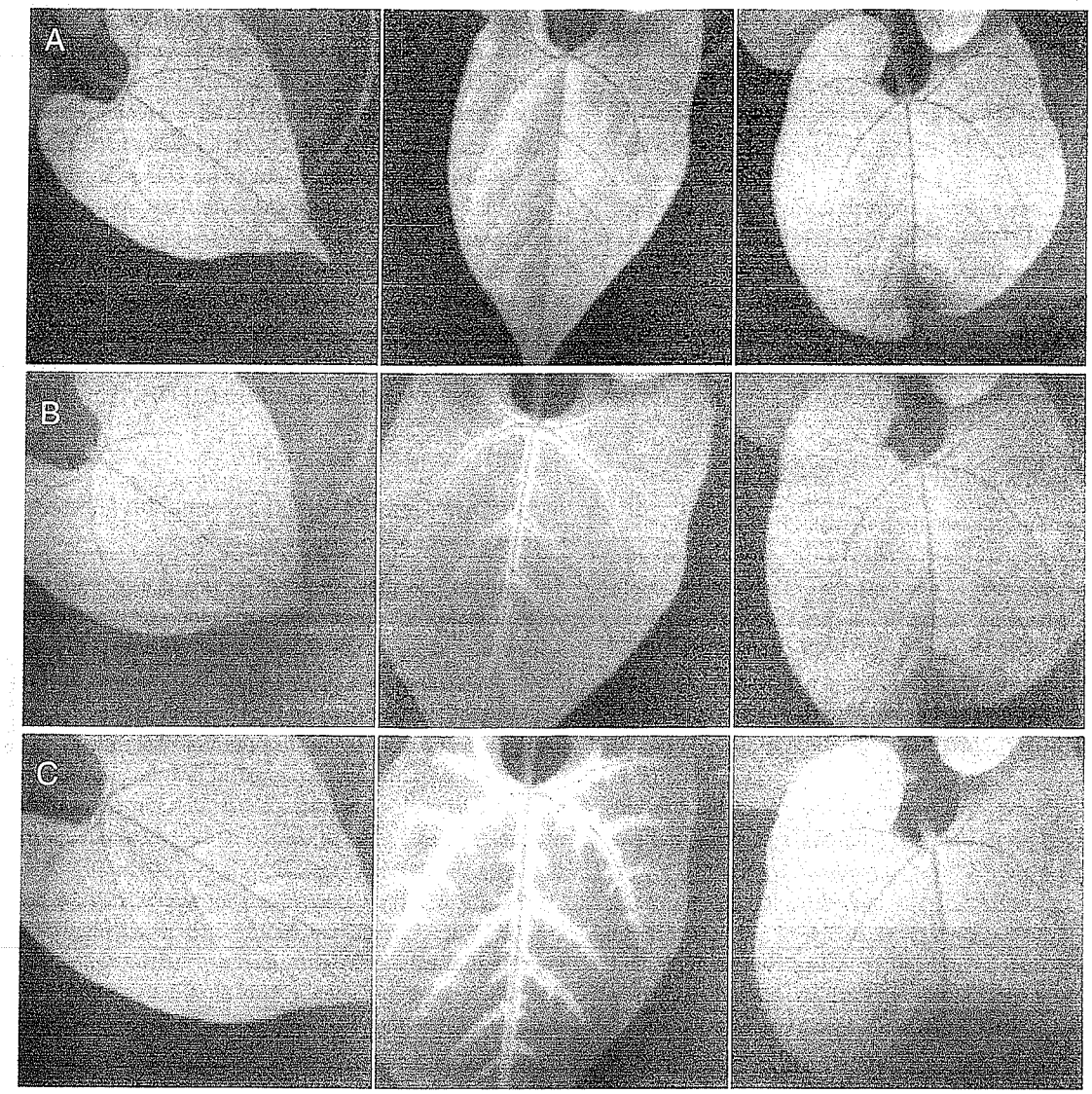


Fig. 10.8. Visualisation of linuron degradation by the bacterial strain *Variovorax paradoxus* WDL1 using multispectral imaging. Images of chlorophyll fluorescence (Chl-F) under excitation light with a photosynthetic photon-flux density of 250 μmol $m^{-2}$ $s^{-1}$ from primary leaves of bean plants. First column, control; second column, leaf treated with the DCMU-like herbicide linuron; last column, linuron+*V. paradoxus*-treated leaf. Leaf sizes increase gradually with time owing to growth expansion. (A) Primary leaves 10 days after planting; (B) images captured after 10 h; (C) images captured 16 h after (A). Modified with permission from Chaerle *et al.* (2003).

In the field of underwater imagery, submersible equipment has investigated the spatial distribution of phytoplankton as well as coral bleaching after recording multispectral images of induced fluorescence (Zawada, 2003).

Chl-FI instruments usually are designed to obtain the two-dimensional maps of standard fluorescence values: $F_0$, $F_0'$, $F_m$, $F_m'$ and $F_s$. To estimate rates and efficiency of the photosynthetic process, $F_v/F_m$, Rfd, $\phi_{PSII}$ and NPQ are calculated for each pixel of the image and presented in a black and white or a false-colour scale (Nedbal and Whitmarsh, 2004; Oxborough, 2004). Nedbal and Březina (2002) have also imaged the harmonically forced oscillations in fluorescence emission to map regulation in light capture. The choice of the adequate fluorescence

parameter to follow a physiological process or to evaluate stress-induced damage depends on the experimental and growth conditions and the stage of plant development, as well as the stress factor analysed (Nedbal and Whitmarsh, 2004). Experimental algorithms that identify the combination of fluorescence parameters provide the highest contrast between different plant samples or segments (Soukupová *et al.*, 2003; Berger *et al.*, 2007; Pineda *et al.*, 2008a,b; see Section 22.8). Some basic statistic tools, such as fluorescence profiles in a given sample and histograms (plotting the number of pixels with selected fluorescence values; Lichtenthaler and Babani, 2000), could also be used to present image data.

### 10.6.2. Multicolour fluorescence imaging

Fluorescence images taken at different spectral bands (multispectral or multicolour fluorescence imaging, MCFI) increase the number of plant processes than can be simultaneously analysed, and provide a promising way to detect specific *signatures* for a particular stress (Lenk *et al.*, 2007). The excitation of leaves with long-wavelength UV radiation (320–400 nm) results in four characteristic fluorescence bands with peaks near to 440 nm (blue; F440), 520 nm (green; F520), 690 nm (red; F690) and 740 nm (FR; F740). BGF is not evenly distributed over the leaf area, but primarily emanates from the main and side veins. In contrast, the red and FR Chl-F is predominantly emitted from the vein-free leaf regions (Lichtenthaler and Miehé, 1997). The use of the fluorescence ratios F440/F520, F440/F690, F440/F740 and F690/F740 is widespread, as BGF and Chl-F have distinct origins and can change independently in response to stress factors and during plant development. F440/F690 and F440/F740 are very early stress indicators and F440/F520 could change after long stress exposure. The F690/F740 ratio presents an inverse relationship with the leaf chl. content (Cerovic *et al.*, 1999; Buschmann *et al.*, 2000). MCFI can provide information about gradients and distribution of the different fluorescence signals related to photosynthetic (Chl-F) and secondary (BGF) metabolism. During the stress response, different phenolic compounds from the phenylpropanoid pathway can accumulate and generally emit BGF after UV excitation (Lichtenthaler and Miehé, 1997; Cerovic *et al.*, 1999). Microscopic studies of UV-induced fluorescence have revealed some of the main BGF emitters and their location in the plant cell as ferulic acid (Morales *et al.*, 1996) or chlorogenic acid (Morales *et al.*, 2005).

Changes in fluorescence ratios and values were analysed in plants suffering under different plant developmental stages (Buschmann *et al.*, 2000; Meyer *et al.*, 2003) and abiotic stress conditions: light (Middleton *et al.*, 2005; Lenk and Buschmann, 2006), drought and temperature (Lichtenthaler and Miehé, 1997), herbicides (Lichtenthaler *et al.*, 2005), as well as mineral deficiencies and excesses (Lichtenthaler *et al.*, 2005).

Multispectral fluorescence and reflectance imaging have been successfully used for classification or sorting of agricultural products (Kim *et al.*, 2003; Ariana *et al.*, 2006), evaluation of UV-screening and activation of the secondary metabolism (Lichtenthaler and Miehé, 1997; Agati *et al.*, 2002).

### 10.6.3. Other related imaging techniques applied to measurements of plant physiology

The ability to collect spatially resolved data for a wide range of molecular, physiological and biophysical processes is increasing dramatically (Chaerle and Van Der Straeten, 2000). Water limitation or other localised changes in leaf chemistry affect stomatal conductance, and thermal imaging offers a powerful tool for mapping changes in temperature associated with variation in latent heat flux across leaf surfaces (Omasa and Takayama, 2003). With proper calibration, thermal maps can be converted directly into maps of stomatal conductance (Jones, 2004a).

A wealth of information about photosynthesis and other aspects of leaf physiology could be obtained by applying complementary imaging methods in the same leaf. Combining different images with different resolution is, however, challenging. One approach is to construct simple regressions between the values in aggregate pixels in one image with aggregate pixels in another image. West *et al.* (2005) applied this approach to an examination of the effect of stomatal patchiness (thermal image) on photosynthesis (fluorescence image). Deeper insight can be gained by applying methods of geographical image analysis to physiological data (Omasa and Takayama, 2003; Leinonen and Jones 2004; Aldea *et al.*, 2006a). By registering and re-sampling images taken with different instruments, different images can be aligned precisely and expressed at a common resolution.

The spatial pattern of other components of the photosynthetic machinery, including chl. content and engagement of the xanthophyll cycle (Gamon *et al.*, 1997), are readily mapped with hyperspectral imaging (Chaerle and Van Der Straeten

2000; Schuerger *et al.*, 2003; Blackburn, 2007), though this has not yet been applied to variation within single leaves.

Highly sensitive cameras now make it possible to image the autoluminescence or ultra-weak spontaneous luminescence owing to oxidative stress and lipid peroxidation in plants (Flor-Henry *et al.*, 2004; Havaux *et al.*, 2006). This new imaging approach enables the screening of mutants with variable tolerance to oxidative stress, as well as following the generation of excited states during stress-induced oxidative reactions (Ohya *et al.*, 2002; Reverberi *et al.*, 2005). Various tracers and dyes also allow mapping ROS (Miller *et al.*, 2005; Flors *et al.*, 2006; Hideg *et al.*, 2006).

Examples of different physiological processes (water and metabolite movement, root–soil–water interactions, gene expression, presence of defence and signalling compounds) that can be monitored remotely *in vivo* with a range of imaging approaches (nuclear magnetic resonance (NMR) imaging, geophysical techniques, use of intrinsically fluorescent proteins, LIDAR imaging) are presented in Chaerle and Van der Straeten (2001), Aldea *et al.* (2006a), as well as in the special issue of Journal of Experimental Botany devoted to *Imaging Techniques for Understanding Plant Responses to Stresses* edited by Jones and Morison (2007).